PEER REVIEWED

Modeling binder migration during drying of a paper coating

PHILIPPE BERNADA AND DENIS BRUNEAU

ABSTRACT

This paper deals with the physical mechanisms that occur during the drying of paper coating. An experimental study on the migration of natural binder (starch) is briefly presented. Using these experimental results, an original model of paper coating drying is validated. This model, which is based on diffusive liquid transport, takes into account the shrinkage of the coating and the migration of the starch during drying. The results of this research lead us to suggest that starch migration occurs until the coating is totally consolidated.

Application:

This problem of starch migration during the drying of a coating is directly linked to the printability and the final quality of the coated paper.

TO IMPROVE THE QUALITY OF A paper base sheet, it can be covered by a coating that is generally a compound of three different elements: water, pigments, and binders. The binders provide good cohesion of the porous structure formed by the pigments. Two kinds of binders are generally used:

- Natural binders, e.g., starch. Because of its strongly absorbent chemical structure, starch has a complex drying behavior that is strongly linked with its moisture content and temperature.

- Synthetic binders, e.g., latex.

During drying, the coating loses moisture and becomes consolidated. During this consolidation process, one can observe three different coating states: *liquid, gel,* and *solid.*

At the beginning of drying, the coating is a two-phase compound with a viscous liquid in which particles with different shapes and dimensions can move. Because of the drying flux and the water penetration into the base paper, liquid tends to flow respectively toward the top surface and the base sheet, carrying binders with it. As drying proceeds, the solid content increases, and the movement of solid components becomes more difficult. In the same time, the coating shrinks. At this stage, the total volume lost by the coating during a given period of time is equal to the volume of water lost by evaporation during this same period. This type of shrinkage is called *total* or *ideal shrinkage.*

At one point of the drying, a bulky but three-dimensional network is formed by binders, and pigments are trapped *(1)*. This point, called the *gel point*, is characterized by a typical moisture content that we denote W_g. This coating characteristic depends on the latex stiffness and on the colloidal interactions that exist between clay platelets and binders. During this phase, capillary forces induce important compressive stresses in the solid structure so that the coating continues to shrink *(1, 2)* (shrinkage is still ideal). Unfortunately, the effect of this structural change on the binder migration is not yet clearly known. Lepoutre and Watanabe state that free motion of latex binders is negligible after the gel point *(1)*, while Lee *et al.* and Hagen consider that natural binders, which are strongly linked to water, could move after the coating reaches the gel point *(3, 4)*.

Because internal stresses increase in the coating, the solid structure becomes more rigid so that at one point of the drying, binders and pigments can no longer move. This point, called the *critical point*, is characterized by another typical moisture content (denoted here by W_c), which depends on the chemical composition of the coating. When the coating surface reaches this point, the evaporation front recedes within the coating. Above this front, the coating is completely solid, and the shrinkage has stopped. Below this front and toward the bottom of the coating, the coating is still a deformable gel.

In paper coating processes, binders may migrate along with the movement of the aqueous phase toward the base paper and the coating surface. That migration causes nonuniform distributions of binders on the coating surface. In fact, binder migration toward the coating surface significantly influences coating surface properties such as porosity and, ultimately, printability. It is thus important to understand these migration phenomena to improve the final paper quality.

In the first part of this paper, the experimental setup for determining both drying kinetics and moisture content profiles is briefly detailed. The outlines of the modeling are then developed in the second section. This leads to the comparison of the numerical and experimental results in terms of moisture content (kinetics, moisture profiles) and starch concentration. Finally, a general summary of the results is proposed.

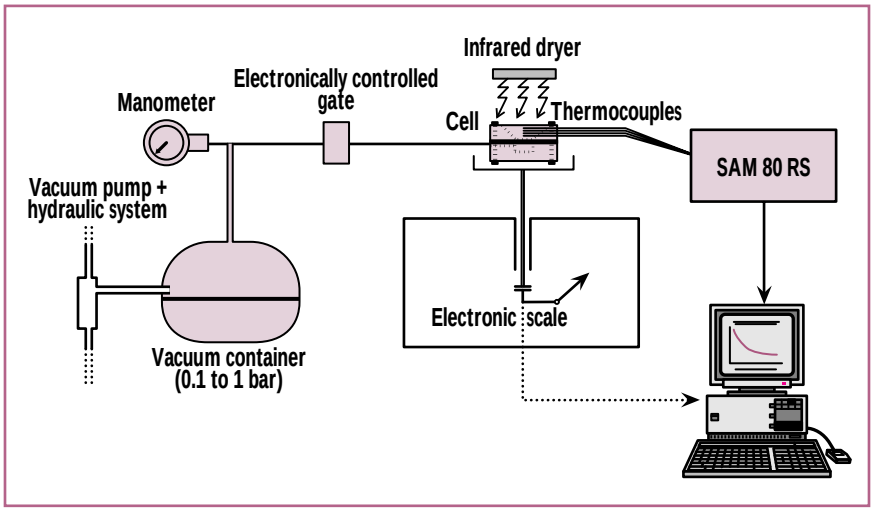

1. Experimental configuration

T_{emit} = 80°C	T_{emit} = 60°C
• If t <9000 s, $F_m^d(t) = A_{80} \exp(B_{80}t) + C_{80} \exp(D_{80}t) + E_{80} \exp(F_{80}t)$	• If t <50 s, $F_m^d(t) = A_{60}$
• If t Œ [9,000, 17,000], $F_m^d(t) = G_{80}$	• If t >50 s, $F_m^d(t) = A_{60} \exp(B_{60}\, t^{C\,60}])$
• If t >17,000 s, $F_m^d(t) = H_{80} \exp(I_{80}t)$	

I. Drying mass flux correlation function

Initial conditions	Moisture content, W_0	0.572
	Mass fraction of starch, W_{a0}	0.02
	Thickness, e_0 (cm)	1
Physical characteristics of the coating	Moisture content at the gel point, W_g	0.315
	Moisture content at the critical point, W_c	0.185
Modeling of the transport coefficient as a function of moisture content, $D(W)$	• If W 0.35: $D(W) = A_L \exp[B_L(W–W_0)]$	
	• If W Œ [0.3, 0.35]: $D(W) = C_L \exp[D_L(W–0.35)]$	
	• If W Œ [0.275, 0.3]: $D(W) = E_L$	
	• If W Œ [0.23, 0.275]: $D(W) = E_L \exp[F_L(W–0.275)]$	
	• If W Œ [0.1, 0.23]: $D(W) = G_L \exp[H_L(W–0.23)]$	
	• If W Œ [0.07, 0.1]: $D(W) = I_L$	

II. Transport parameters and physical characteristics of the coating

EXPERIMENTAL SETUP

The principal goal of this study is to understand and quantify the different phenomena observed during the drying of a paper coating. With this aim in mind, coating samples are studied alone. Nevertheless, the effect of water penetration in the base paper is simulated by an original method. A short description of the experimental setup is given in the following sections. Note: In the following paragraphs, the simulation of water penetration into the base sheet is denoted "dewatering simulation."

Coating formulation

For each drying experiment, the coating formulation is the same. It can be defined, in terms of mass fraction C_i = mass of component i/total mass of the wet coating, as follows:

- Hydrocarb (carbonates): C_c = 27%
- a-gloss (kaolins): C_k = 27%
- Latex: C_{lat} = 8%
- Starch: C_s = 3%
- Liquid (water): C_L = 35%.

Drying and dewatering

To reproduce the coating dewatering, a liquid flux toward the bottom of the coating was created by imposing vacuum conditions at the lower boundary of the coating sample. The complete experimental setup (drying and dewatering) is shown in Fig. 1. The setup includes:

- An infrared dryer with adjustable temperature (50–160°C)
- The measure cell (with a porous bottom), which contains the coating samples (Fig. 2)
- A bell-shaped vacuum container that is linked to a hydraulic system which allows a low pressure (0.1 bar) to be obtained
- An electronically controlled gate that works as a switch, allowing (or not allowing) the low pressure under the coating to be established
- An accurate electronic scale (accuracy: ±0.001 g) that gives the evolution of the cell mass during drying
- Acquisition software, which allows the acquisition of the global mass and temperature at various points in the coating.

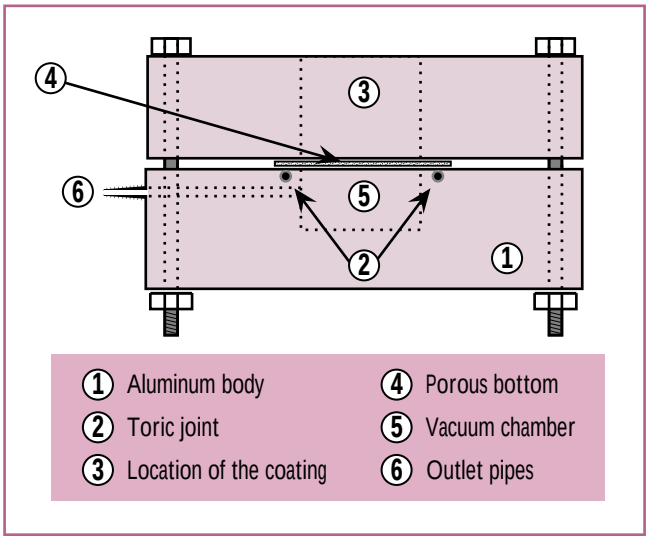

2. Schematic of the experimental cell used for the laboratory coating drying experiments

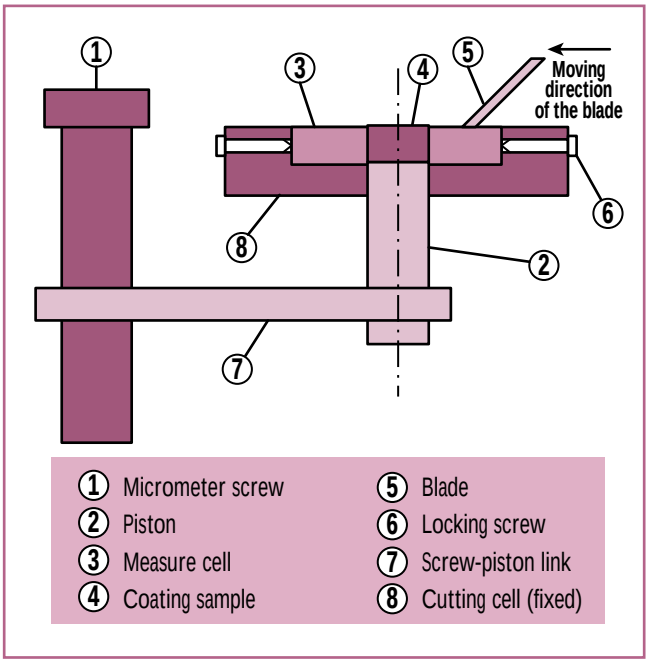

3. Coating cutting configuration

The thickness of the samples (1 cm) is intentionally much greater than that used in industrial processes (approx. 20 µm). This is because determining moisture content or starch content profiles requires cutting the samples to slices, which cannot be executed on very thin coatings.

By imposing a large pressure difference (0.9 bar) between the top of the coating, which is at ambient pressure, and the vacuum chamber in the measure cell, the mass transfers between the coating and this chamber are greatly increased. Consequently, the evaporation flux at the bottom of the coating, which is nearly zero when dewatering is not simulated, becomes important when it is simulated.

Method of determining the moisture content profiles

To characterize the liquid transport in the coating during drying, an experimental process has been developed to determine the moisture content profiles. It is based on a destructive cutting method described in Fig. 3.

At first, the coating is put in the drying experimental setup that was described earlier. At a given time, the drying experiment is stopped and the measure cell is immediately placed and supported in the cutting system by two locking screws. A piston, whose position is located with a micrometer screw, allows the sample to be moved vertically with great accuracy and thus determines the thickness of the slice that is cut by the blade. Twelve slices are generally obtained in 1 cm. Every slice is weighed and placed in an oven at 80°C for 24 hours for complete dehydration. Then, the moisture content of a slice *i* is given by the following equation:

$$W_i = (m_i - m_{di}) / m_{di} \qquad (1)$$

where m_i and m_{di} are the humid mass of the slice and the mass of the dehydrated slice, respectively.

The cutting operation is fast enough that the mass of evaporated

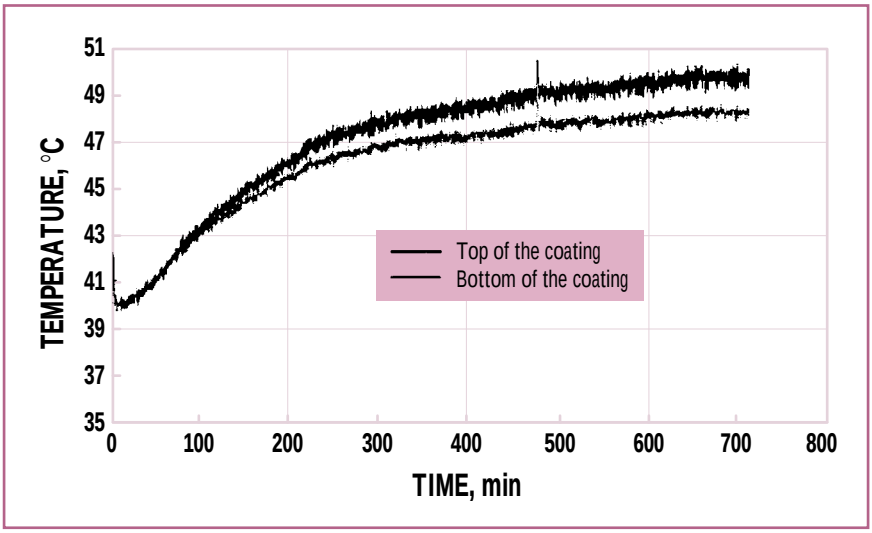

4. Evolution of the temperature at the top and bottom of the coating; a 60°C drying experiment without dewatering simulation.

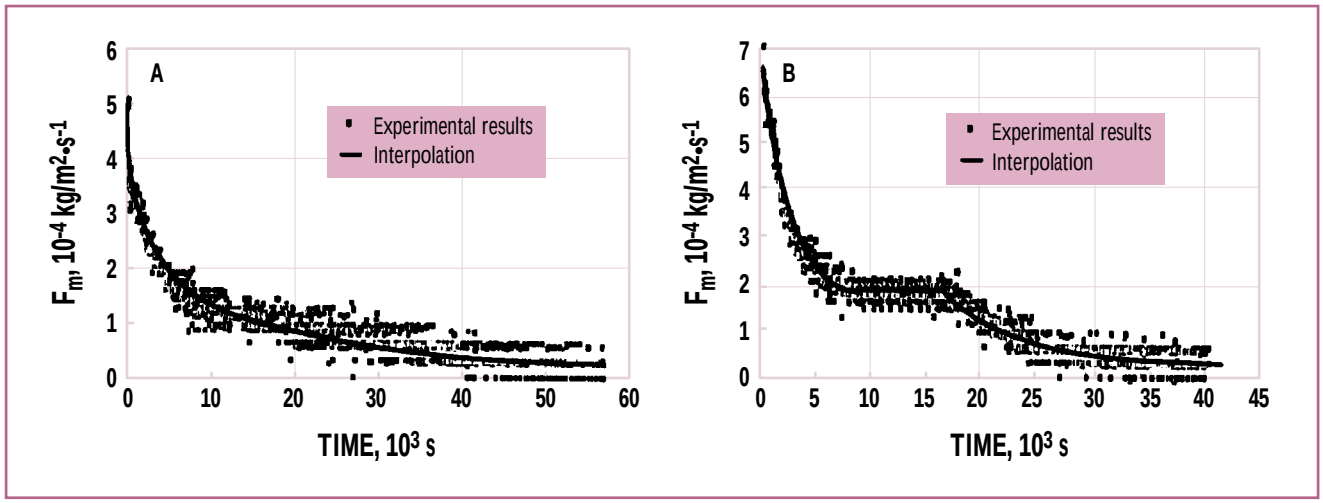

5. Evolution of the mass flux as a function of time—experimental results and interpolation. (a) a 60°C drying experiment without dewatering simulation; (b) an 80°C drying experiment without dewatering simulation.

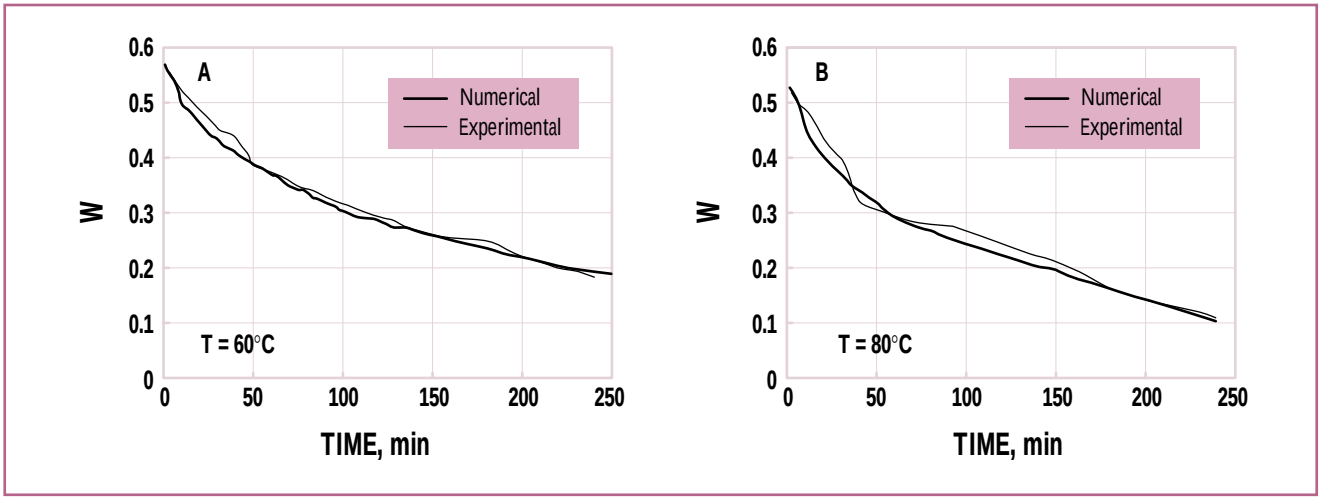

6. Comparison of experimental and numerical drying kinetics. (a) a 60°C drying experiment with dewatering simulation; (b) an 80°C drying experiment with dewatering simulation.

water during cutting and weighing is considered negligible compared to the mass lost during drying.

MODELING

In the first part of this paper, the following physical processes, which occur during coated paper drying, have been described:

- Binder migration (in particular starch) toward the top surface and the base sheet
- Consolidation and shrinkage of the coating structure.

Furthermore, those local physical phenomena depend strongly on the evaporation rate at the surface of the coating and on the flux of water at the coating–base sheet interface.

In the literature, two authors *(5, 6)* have developed models for binder migration. Unfortunately, in each of those models, the coating was assumed to be a rigid, consolidated porous medium with a fixed permeability, even if the coating remained fluid.

In this paper, an original model of a coating drying process is proposed. It takes into account binder migrations, the consolidation process, and shrinkage of the coating in the coupled differential equations. Evaporation and dewatering rates, which control the drying process, are simply expressed in the boundary condition equations.

The main assumptions of the model

Assumption 1. The intrinsic density of the solid phase, ρ, is assumed constant and is defined by:

$$\rho = \frac{1}{\phi} \sum_i \rho_i \phi_i \qquad (2)$$

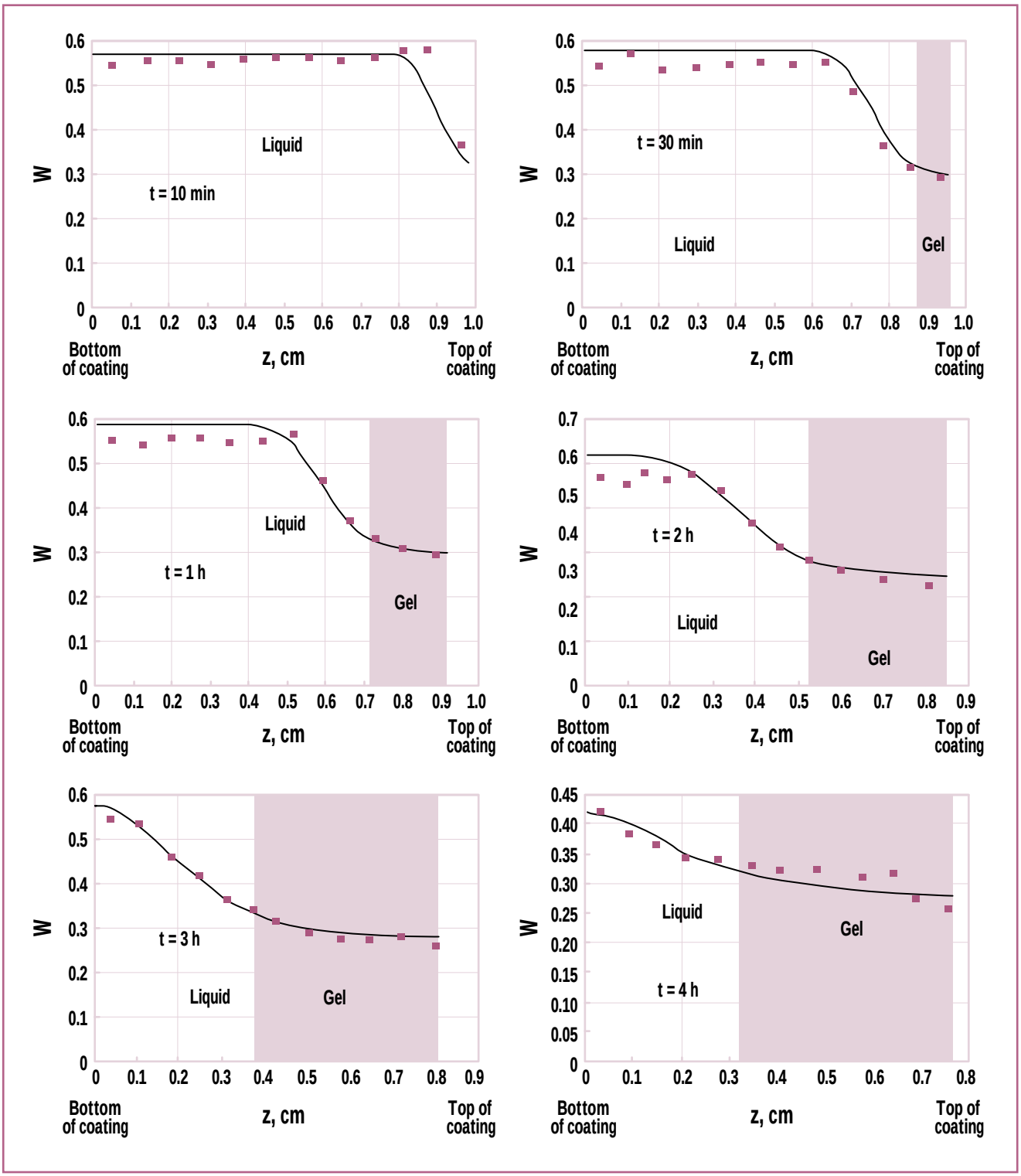

7. A 60°C drying experiment without dewatering simulation; comparison between numerical (continuous line) and experimental (points) moisture content profiles at different stages of the drying experiment.

where f, r_i, and f_i are the solid volume fraction of the total solid phase (defined in Eq. 9), the intrinsic density, and the volume fraction of a particular type of solid component *i*, respectively. In reality, starch migrations in the coating modify the intrinsic density. But as a consequence of the low starch volume fraction in the tested coating (2%), the variations of solid density due to those migrations can be considered negligible.

Assumption 2. During the drying process, the coating is assumed to be

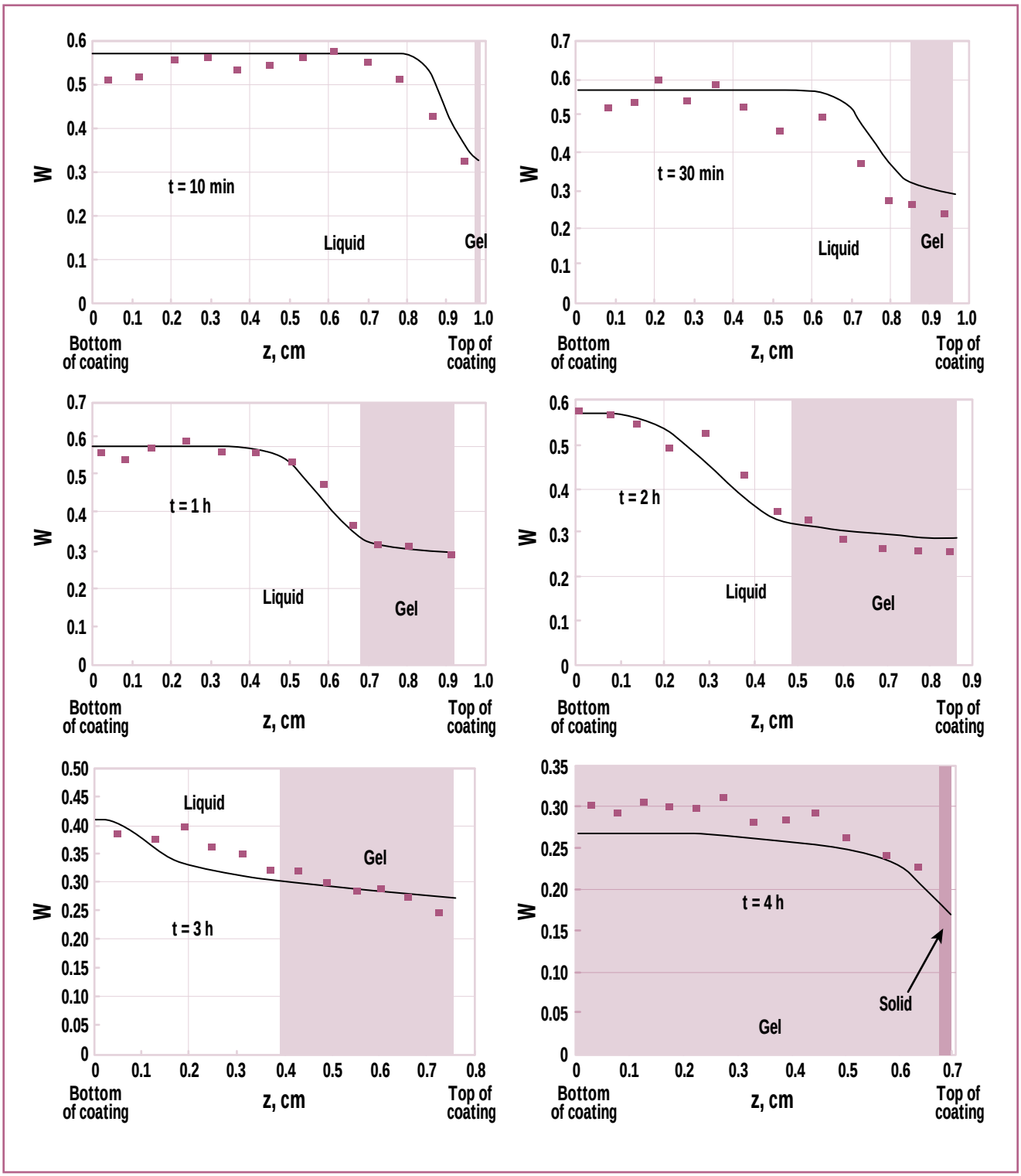

8. An 80°C drying experiment without dewatering simulation; comparison between numerical (continuous line) and experimental (points) moisture content profiles at different stages of the drying experiment.

isothermal. This hypothesis, which has been verified in the case of a thin industrial coating, could here be extended to thick layers (Fig. 4). In fact, temperature measurements in the coating during drying show that thermal gradients between the top and bottom of the coating appear to be negligible (2°C at the most).

Set of equations

In the coupling of shrinkage and consolidation processes during the drying of a coating, the coating is considered to dry in two stages:

before and after the critical point.

Before the critical point, as the local moisture content is greater than W_c (critical moisture content), the coating is a two-phase medium, composed only of water and solid particles of different types. The solid volume fraction, f, is then linked to the liquid volume fraction, f_L, or the moisture content, W, by the following equation:

$$f = 1 - f_L$$
$$W = [r_L(1 - f)]/rf \qquad (3)$$

Moreover, if we assume that the shrinkage is total, we can write the following:

$$fV_{shr} + f_L V_L = 0 \qquad (4)$$

where V_{shr} represents average solid-phase velocities (and is defined in Eq. 9) and V_L is the liquid-phase filtration velocity.

After the critical point ($W<W_c$), the evaporation front recedes into the coating and the gaseous phase takes place in the coating. At the same time, the shrinkage of the now-three-phase region becomes zero.

Thus, the modeling presentation is naturally divided into two parts: $W>W_c$ and $W<W_c$.

If $W>W_c$

Writing the mass balance equations. The mass balance equations of the different coating components can be written as follows:

[SEE PAGE 143 FOR EQ. 5]

[SEE PAGE 143 FOR EQ. 6]

$$f_{gas} = 0 \qquad (7)$$

where r_i and V_i are, respectively, the density and velocity of a solid component i, n is the number of solid components in the coating (carbonates, kaolins, latex, starch), and f_{gas} is the gas volume fraction.

By making the sum for i equal 1 to n, we write the global mass balance equation for the total solid phase as follows:

$$(\partial/\partial_t)(f) + (\partial/\partial_z)(fV_{shr}) = 0 \qquad (8)$$

where f and V_{shr} are defined by:

$$\phi = \sum_{i=1}^{n} \phi_i$$

$$\phi V_{shr} = \sum_{i=1}^{n} \phi_i V_i \qquad (9)$$

Modeling the velocities. The goal of the previous mass balance equations is to obtain numerical simulations of the time evolution of moisture content and starch profiles in the coating. Therefore, we now write a model for the velocity of the liquid, the average velocity of solid components, and the velocity of starch.

Because the internal structure of the coating during drying is not well known, a diffusive model for the liquid-phase velocity is chosen. Using the definition of the total shrinkage *(7)*, V_L and V_{shr} can be expressed as a function of the gradient of liquid or solid volume fraction:

[SEE PAGE 143 FOR EQ. 10]

where $D(f)$ is the global transport coefficient, which strongly varies with the liquid volume fraction.

The starch velocity modeling has been developed according to the fact that starch is strongly linked to water; thus, the relative velocity to the mean solid movement can be written as follows:

$$V_{s(rel)} = V_{s(abs)} - V_{shr} =$$
$$(V_L - V_{shr})\, f(f) \qquad (11)$$

where $V_{s(abs)}$ and $V_{s(rel)}$ are, respectively, the absolute and relative starch velocity, and $f(f)$ is a factor that varies with and takes into account the reducing action of the other particles of the starch movement during drying. The expression of this factor is discussed later in "Results and discussion."

Changing the space coordinates. The modeling equations of liquid transport and starch migration during drying have been established (Eqs. 5, 6, 10, and 11). The numerical solution of these equations, written here in aileron coordinates, proves difficult because of the coupling between drying and shrinkage. We thus choose to rewrite them in the solid-based coordinate z_0. The particularity of this type of coordinate is to be attached to a mass element of solid and, thus, the shrinkage terms are no more apparent in the equations.

This section presents the calculations that allow us to transform the mass balance equations from the aileron to the solid-based coordinates system. These calculations lead to the equations that have been solved to obtain numerical results for the modeling presented previously. They are not described in details here. Further details can be found in Ketelaars *(8)* and Zagrouba *(7)*. The transformation equations are:

$$\left.\frac{\partial}{\partial t}\right|_{z_0} = \frac{d}{dt} = \left.\frac{\partial}{\partial t}\right|_{z} + V_{shr}\left.\frac{\partial}{\partial z}\right|_{t}$$

$$\left.\frac{\partial}{\partial z_0}\right|_{t} = \frac{\phi_0}{\phi}\left.\frac{\partial}{\partial z}\right|_{t} \qquad (12)$$

in which f_0 is the initial solid volume fraction. By using the variables W and C_s (defined in Eqs. 14a and 14b) instead of f_L and f_s (starch volume fraction), one can transform the equation for liquid (Eq. 5) and the equation for starch (Eq. 6) from the aileron coordinate system to the solid-based coordinate system. After some calculations, we obtain the following *(9)*:

$$\frac{\partial W}{\partial t} - \frac{\partial}{\partial z_0}\left[D_{eff}(W)\frac{\partial W}{\partial z_0}\right] = 0 \qquad (13a)$$

$$\frac{\partial C_s}{\partial t} - \frac{\partial}{\partial z_0}\left[C_s V_{eff(s)}(W)\right] = 0 \qquad (13b)$$

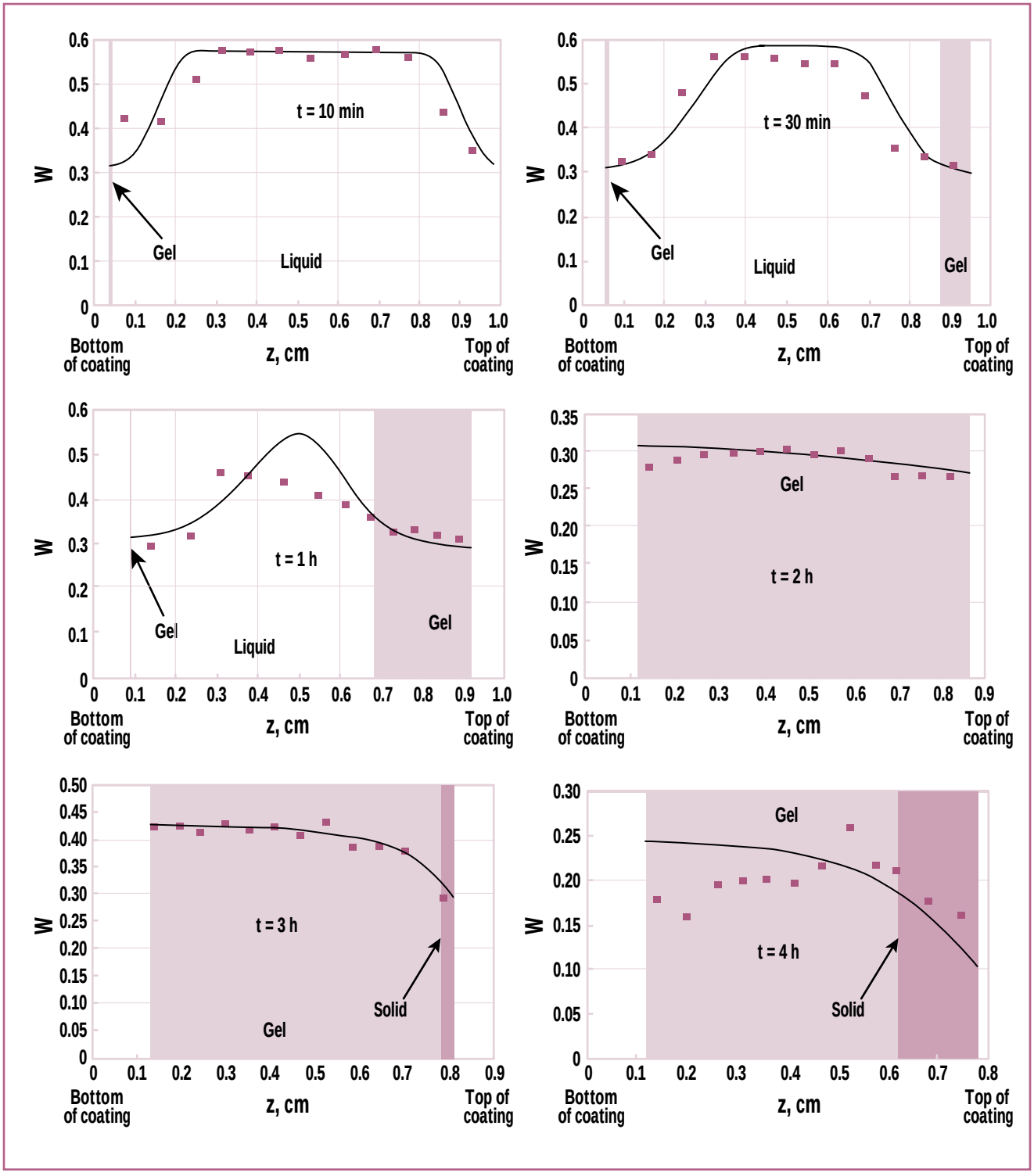

9. A 60°C drying experiment with dewatering simulation; comparison between numerical (continuous line) and experimental (points) moisture content profiles at different stages of the drying experiment.

where

$$W = (r_L f_L)/rf \qquad (14a)$$

$$C_s = (r_s f_s)/rf \qquad (14b)$$

[SEE PAGE 143 FOR EQ. 15a]

[SEE PAGE 143 FOR EQ. 15b]

and W_0 is the initial moisture content.

If $W<W_c$

In this case, the solid matrix is rigid, and the global mass balance equation for the solid phase becomes:

$$f = f_c \qquad (16)$$

where f_c represents the solid volume fraction at the critical point.

In a consolidated region, the local starch mass fraction (defined in Eq. 14b) remains constant and equal to the value it has reached when this region becomes consolidated. This value depends on the position of the coating in the consolidated region and is a consequence of the starch migration before consolidation. This can formally be written as follows:

$$C_s = cst(z) \qquad (17)$$

In contrast to the mass balance equations (Eqs. 16 and 17), the governing set of equations for the moisture transport are not trivial:

[SEE PAGE 143 FOR EQ. 18]

where ρ_v and V_v are, respectively, the density and velocity of the vapor; ρ_{da} and V_{da} are, respectively, the dry air density and velocity; and K_e is the rate of evaporation *(9, 10)*.

At first, this case ($W < W_c$) seems to be more complicated than the previous case ($W > W_c$) because of the gas equations. However, in the low-temperature drying conditions that we used, the effects of pressure and temperature are negligible, and the complete model written previously can be reduced to a diffusive model *(10)*. Then, the moisture transport equations (Eqs. 18a and 18b) reduce to the following single equation:

$$\rho_L f_L V_L + \rho_v f_{gas} V_v = -\rho f_c D(W)(\partial W/\partial z) \qquad (19)$$

that is:

$$\frac{\partial W}{\partial t} - \frac{\partial}{\partial z}\left(D(W)\frac{\partial W}{\partial z}\right) = 0 \qquad (20)$$

or in solid-based coordinates:

$$\frac{\partial W}{\partial t} - \frac{\partial}{\partial z_0}\left(D_{eff}(W)\frac{\partial W}{\partial z_0}\right) = 0 \qquad (21)$$

where W and $D_{eff}(W)$ are now defined by:

[SEE PAGE 143 FOR EQ. 22]

By neglecting the small mass contribution $\rho_v f_{gas}$ in the definition of moisture content (Eq. 22), we calculate the gas volume fraction using the moisture content W as follows:

[SEE PAGE 143 FOR EQ. 23]

Finally, Eqs. 17, 21, and 23 lead to obtaining C_s, W, and f_{gas} in the consolidated region of the coating.

Boundary conditions

At the upper limit of the coating. One of the goals of this model is to compare its numerical results to the experiments. But because of the complexity of the dryer geometry and the lack of information on the relative humidity that takes place in the dryer, the mass flux at the upper limit [$H(t)$] of the coating cannot be easily modeled. That is why this flux is chosen as a simple function of time $F_m^d(t)$ derived from the experimental kinetics. Thus, the drying boundary condition finds expression in a mass flux continuity condition:

$$\rho_L f_L (V_L - V_{shr})_{z = H(t)} = F_m^d(t) \qquad (24)$$

Using Eqs. 10 and 12, this flux boundary condition, transformed in solid-based coordinates, becomes:

[SEE PAGE 143 FOR EQ. 25]

where H_0 is the initial position of the upper limit of the material.

In the case of starch, the natural boundary condition that seems plausible to impose is a relative velocity (Eq. 11) equal to zero for a starch particle:

$$V_{s(rel)}\Big|_{z_0 = H_0} = 0 \qquad (26)$$

At the bottom of the coating. If dewatering is not simulated. The mass flux is equal to zero at this interface ($z_0 = 0$), and the natural boundary condition is given in solid-based coordinates by:

$$-\rho\,\phi_0\left[D_{eff}(W)\frac{\partial W}{\partial z_0}\right]_{z_0 = 0} = 0 \qquad (27)$$

If dewatering is simulated. In the experimental setup, dewatering is simulated by creating a depression under the coating sample, through a rigid absorbent membrane. By imposing this depression, a total pressure gradient arises between the top and bottom of the coating; this results in a liquid transport toward the bottom sample. At the same time, the high intensity of the thermal and mass transfer due to the pressure drop, coupled with the low liquid transport properties in the coating, induces a sudden drop in the moisture content at the coating–membrane interface. In a few seconds, the moisture content reaches an equilibrium value of about 0.32 (which squares with the gel point) *(9, 11)*. Later, when the vacuum period is finished (after 1 hour), the mass flux at the bottom of the coating is nearly zero. Thus, in terms of modeling, these experimental results provide the following boundary condition (in solid-based coordinates):

[SEE PAGE 143 FOR EQ. 28]

For the mass conservation of starch, the boundary condition at the bottom of the coating is the same as the one imposed at the top of the coating.

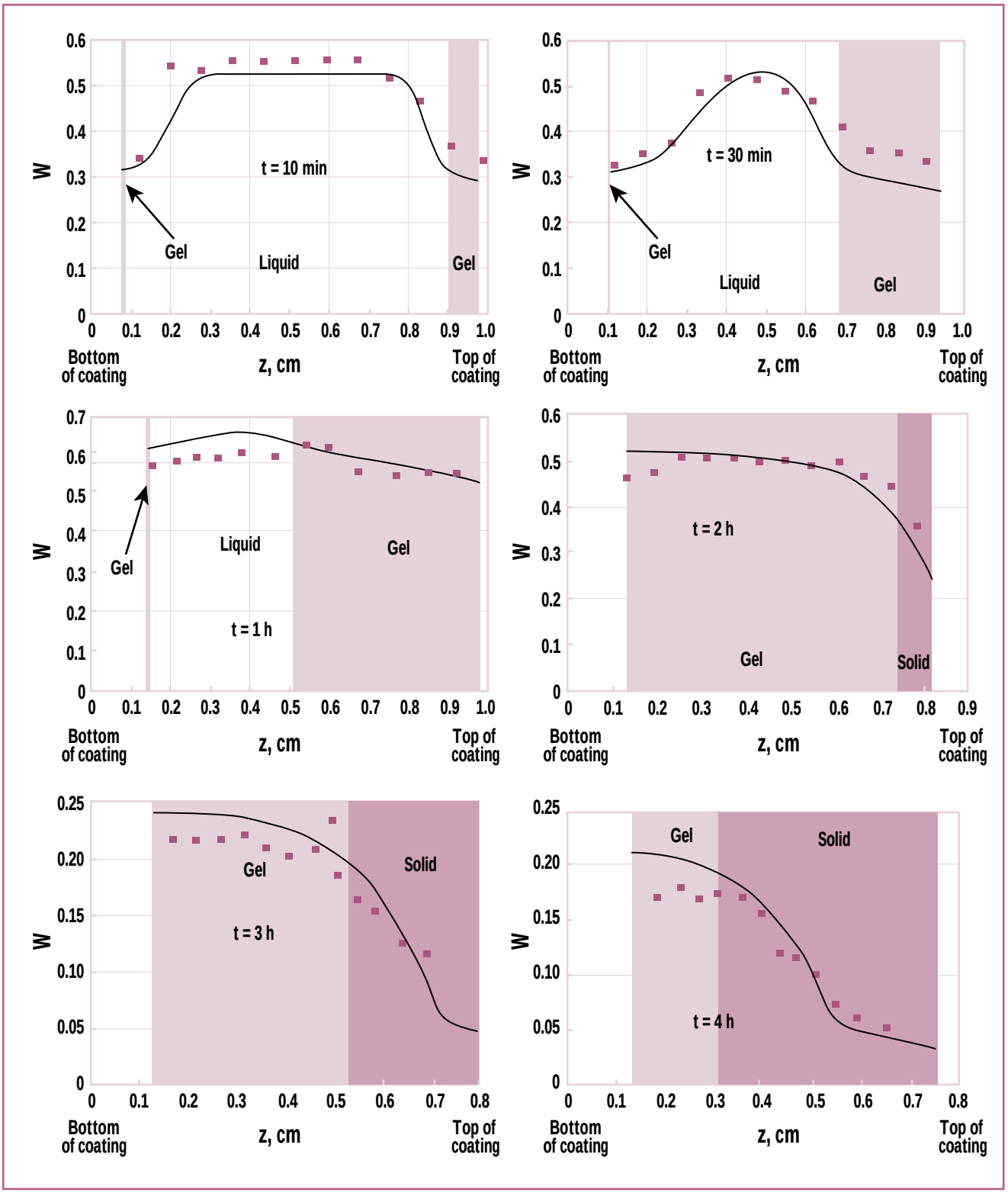

10. An 80°C drying experiment with dewatering simulation; comparison between numerical (continuous line) and experimental (points) moisture content profiles at different stages of the drying experiment.

RESULTS AND DISCUSSION

Resolution parameters. To validate the model, some drying simulations have been performed corresponding to the following two experimental drying temperatures: 60 and 80°C. The internal parameters of the code are given in Tables I and II.

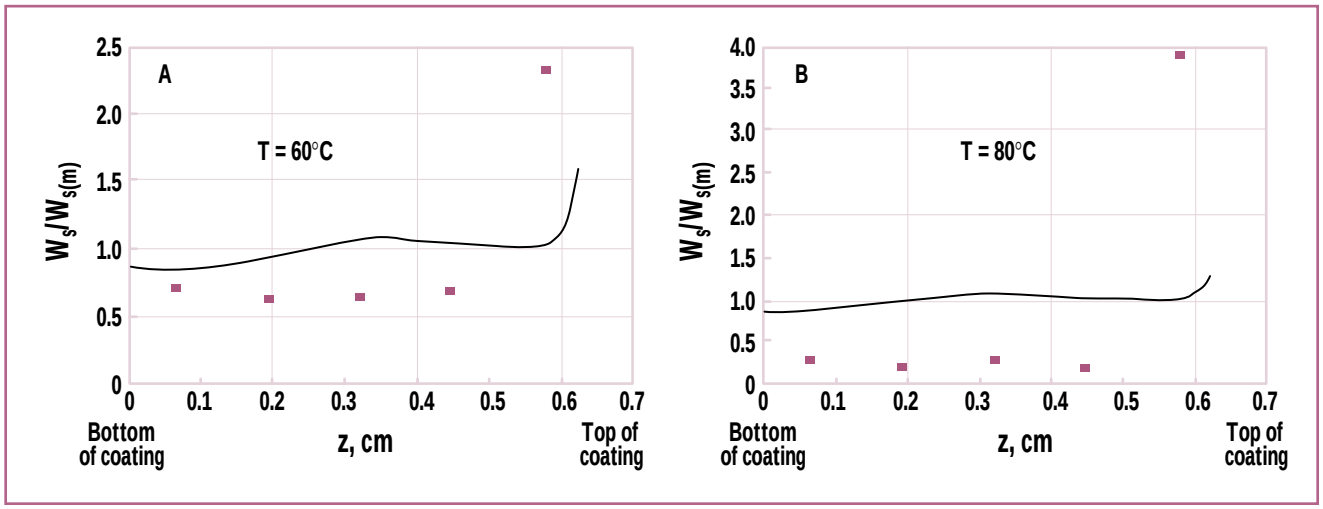

11. Comparison between numerical (continuous line) and experimental (points) starch concentration profiles at the end of a drying experiment. The migration model considers there that migrations can occur until the gel point is reached. (a) a 60°C drying experiment without dewatering simulation; (b) an 80°C drying experiment without dewatering simulation.

The mass flux is calculated from the experimental drying kinetics and interpolated as shown in Fig. 5. The physical properties of the coating (gel point and critical point) have been obtained by applying a graphical approach to the evolution of the moisture content profiles *(9, 11)*. The functional form of the transport coefficient function $D(W)$ has been determined by using the continuity of liquid flow equation at the upper limit of the coating (Eq. 24) and the moisture content profiles for a large series of experiments *(9, 12)*.

Numerical method

The numerical method used to solve Eq. 13a or 21 is a finite element method, with P1 elements. Simultaneously, Eq. 13b is solved by using a finite difference method, which features a one-order up-stream scheme.

Drying kinetics

The mass flux introduced in the model as a boundary condition is directly deduced from experimental kinetics so that if dewatering is not simulated, numerical and experimental kinetics are identical. However, if dewatering is simulated, the boundary condition for the moisture content at the bottom of the coating is the Dirichlet type for the period of 1 hour (Eq. 28). This boundary condition could, in principle, affect the macroscopic kinetics. The comparison between experimental and numerical kinetics is shown in Fig. 6 for the two drying configurations with dewatering. The results show that experiments and numerical simulations are in good agreement over the range of the tested moisture contents and temperatures. So, without imposing the mass flux at the bottom of the coating, the Dirichlet boundary condition preserves the general aspect of the macroscopic kinetic.

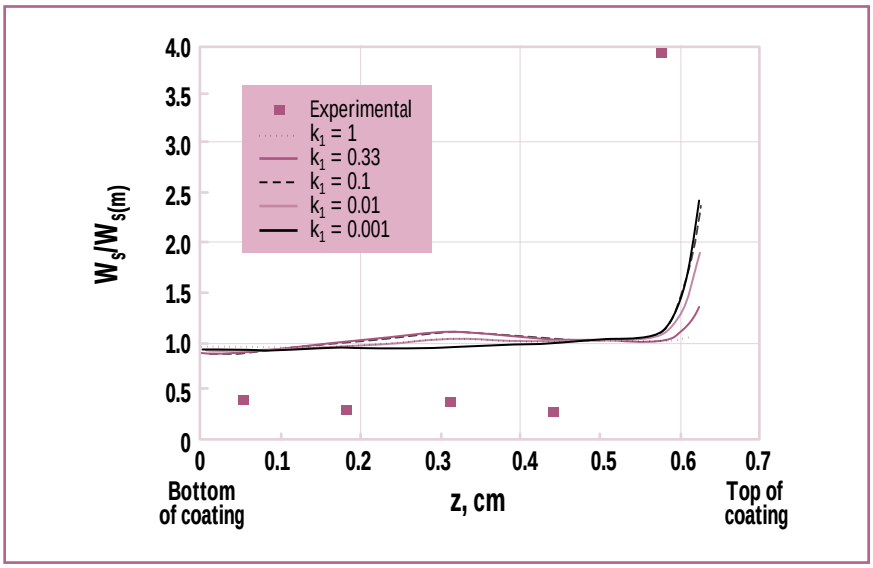

12. Numerical (continuous line) and experimental (points) starch concentration profiles for an 80°C drying experiment without dewatering simulation (k_1 factor influence on numerical results)

Moisture content profiles

Figures 7–10 represent the evolution of moisture content profiles obtained by experiments (black square points) and numerical calculations (continuous line). On each figure, the state of the structure is represented by regions drawn with different shades: white (liquid state), light gray (gel state), and dark gray (solid state).

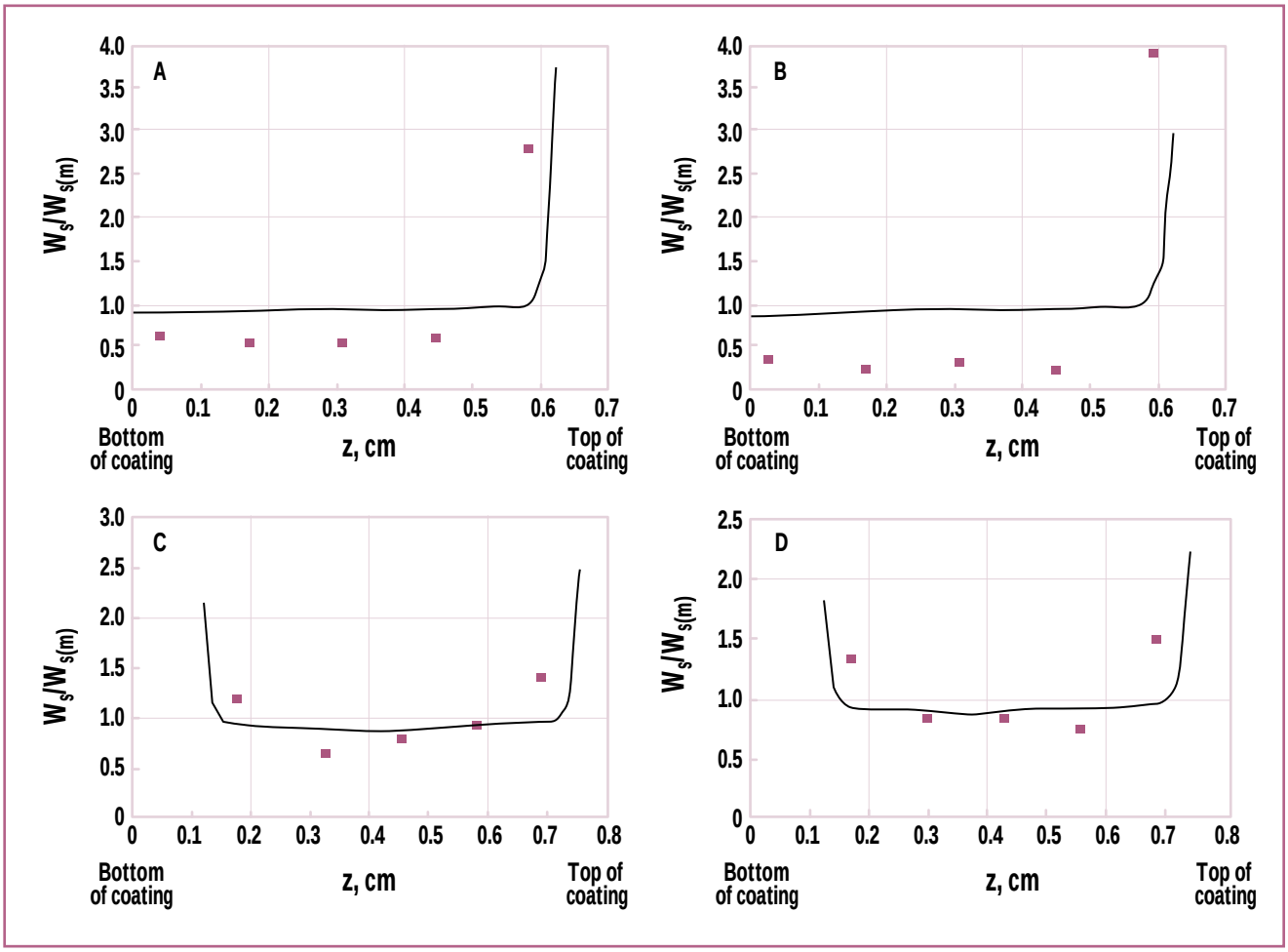

13. Comparison between numerical (continuous line) and experimental (points) starch concentration profiles at the end of a drying experiment. The migration model considers there that migrations can occur until the critical point is reached. (a) a 60°C drying experiment without dewatering simulation; (b) an 80°C drying experiment without dewatering simulation; (c) a 60°C drying experiment with dewatering simulation; (d) an 80°C drying experiment with dewatering simulation.

In the four configurations, numerical simulations and experimental results are in good agreement. Thus, as the transport coefficient is the same in the different simulations, for the temperature scale used here, the transport phenomena are independent of temperature.

As previously noted, the gel point can be deduced from the moisture content profiles. For example, consider the inclined part of the first moisture content profile in Fig. 7. To the right of the lower limit of this portion of the curve, the coating structure is gel, and to the left, the coating is still liquid. The approximate value for the moisture content at the gel point is found in Fig. 7, and for any experiment, $W_g \approx 0.32$. The rough slope change of the profiles below the gel point is due to the sudden increase of the transport coefficient during the transition from liquid to gel. This phenomenon results from the superposition in the gel of a liquid transport due to solid matrix shrinkage with the classical transport by the moisture content gradient *(12, 13)*.

When dewatering is simulated, the agreement between experiments and simulations remains good. This result confirms the choice of the model proposed for the boundary condition at the lower limit of the coating. One can see the considerable effect of dewatering, not only on the moisture content profiles but also on the total drying rate. The second change of structure at the upper limit of the coating (gel–solid) now occurs quite rapidly (3 and 2 hours, respectively, for drying temperatures of 60 and 80°C).

Starch content profiles at the end of drying

To determine starch migration during drying, we have first modeled the starch velocity by Eq. 11, where the factor $f(f)$ is defined as follows:

[SEE PAGE 143 FOR EQ. 29]

in which f_g represents the solid volume fraction at the gel point. In this case, we consider that starch migration decreases with increasing solid content and is stopped when the coating reaches the gel point. This

KEYWORDS
Adhesive migration, binders, coating, consolidation, critical point drying, dry process, drying, equations, experimental design, gels, kinetics, mathematical models, models, moisture content, shrinkage, simulation, starch, velocity, water removal.

assumption has been experimentally verified for latex *(1)* and is extended here to starch. To express a volumetric effect of the factor on the starch velocity, we first choose the value 1/3 for k_1.

The numerical and experimental results are represented in Fig. 11 for two drying configurations without dewatering simulation (60 and 80°C). In this figure, W_{ms} represents the mean value of the starch content in the final thickness of the coating.

Unfortunately, the numerical and experimental results do not agree in Fig. 11. In particular, the experimental starch concentration value at the top of the coating is very high for both configurations while the numerical value remains low.

To improve the quality of these numerical results, we tried to modify the function $f(\mathrm{f})$ and at first the power k_1 in Eq. 29. The results of this study are indicated in Fig. 12. Even for very low values of k_1, the numerical results do not match the experimental ones.

In the other solution we chose to improve, the starch migration model consists of extending the starch migration until the critical point is reached. This can be done by replacing f_g by f_c in Eq. 29; furthermore, we modify the power k_1. The new function $f(\mathrm{f})$ is now:

[SEE PAGE 143 FOR EQ. 30]

This assumption is close to the one used by Lee and Whalen-Shaw *(4)*, who believe that some of the binders can move after the immobilization point. In particular, natural binders like starch are strongly linked to water because of their chemical and physical properties. Thus, the starch migration up to the consolidation point seems to be close to reality.

To confirm this assumption, the comparison between numerical simulation, using Eq. 30, and experimental results is given in Fig. 13 for several drying configurations. In both qualitative and quantitative ways, the numerical profiles are now in good agreement with the experiments. An important part of the starch is driven toward the bottom of the coating by the water flow due to the dewatering. Another portion is carried out toward the top of the coating due to the drying flux.

CONCLUSIONS

A mathematical model has been developed for the simulations of starch migration in a coating paper. This modeling takes into account the shrinkage and consolidation of the coating during drying. The starch velocity is assumed to be the sum of a mean solid velocity and a relative velocity that is strongly coupled to the liquid-phase velocity and the solid volume fraction.

A numerical code based on the modeling has been performed. In a moisture transport term, the numerical results are in good agreement with the experimental ones. In a starch migration term, the results show that starch migration goes on after the gel point.

As a result of this study, the principal perspective on the model is to integrate more physical insight into the determination of the starch velocity. In particular, a solid particle interaction model is now being developed to improve the actual factor $f(\mathrm{f})$. TJ

Bernada is a professor and Bruneau is an assistant professor at Laboratoire Energétique et Phénomènes de Transfert, Esplanade des Arts et Métiers, 33405 Talence, France.

Received for review Oct. 2, 1995.
Accepted May 8, 1996.

LITERATURE CITED

1. Lepoutre, P. and Watanabe, J., *J. Appl. Polymer Sci.* 27(11): 4207(1982).
2. Brinker, C. J. and Scherer, G. W., *Sol-Gel-Science, The Physics and Chemistry of Sol-Gel Processing,* Academic Press, San Diego, 1990, pp. 416-417.
3. Hagen, K. G., *Binder migration in paper and paperboard coatings,* TAPPI PRESS, Atlanta, 1993, pp. 39–59.
4. Lee, D. I. and Whalen-Shaw, M., *Binder migration in paper and paperboard coatings,* TAPPI PRESS, Atlanta, 1993, pp. 19–38.
5. Farkas, I., Lampinen, M. J., and Ojala, K., *Drying Technology* 9(4): 1019(1991).
6. Nowicki, S. C., Davis, H. T., and Scriven, L. E., *Binder migration in paper and paperboard coatings,* TAPPI PRESS, Atlanta, 1993, pp. 1–18.
7. Zagrouba, F., "Séchage mixte par convection et un apport rayonnant micro-onde des milieux déformables. Modélisation des phénomènes de transferts de chaleur et de matière," Ph. D. thesis, National Ploytechnic Institut of Lorraine, Nancy, France, 1993.
8. Ketelaars, A. A. J., "Drying deformable media: kinetics, shrinkage and stresses," Ph. D. thesis, University of Eindhoven, Eindhoven, The Netherlands, 1993.
9. Bernada, P., "Analyse expérimentale et modélisation de la migration des liants dans une couche papetière soumise à un flux de séchage," Ph.D. thesis, Nationale Supérieure des Arts et Métiers, Bordeaux, France, 1995.
10. Nadeau, J. P. and Puiggali, J. R., *Séchage: des processus physiques aux procédés industriels,* Lavoisier, Tech. et Doc., Paris, 1995, pp. 31, 39.
11. Bernada, P. and Bruneau, D., *Revue de Physique III,* in press.
12. Auria, R., Contribution à l'étude du séchage naturel: structure interne et transfert d'humidité lors du séchage, Ph. D. thesis, University of Sciences and Technics of Languedoc, Montpellier, France, 1988.
13. Gehrmann, D. and Kast, W., *Proceedings of the First International Drying Symposium,* Science Press, Princeton, 1978, p. 239.

EQUATIONS

$$\frac{\partial}{\partial t}\left(\rho_L \phi_L\right) + \frac{\partial}{\partial z}\left(\rho_L \phi_L V_L\right) = 0 \Rightarrow \frac{\partial}{\partial t}\left(\phi_L\right) + \frac{\partial}{\partial z}\left(\phi_L V_L\right) = 0 \qquad (5)$$

$$\frac{\partial}{\partial t}\left(\rho_i \phi_i\right) + \frac{\partial}{\partial z}\left(\rho_i \phi_i V_i\right) = 0 \Rightarrow \frac{\partial}{\partial t}\left(\phi_i\right) + \frac{\partial}{\partial z}\left(\phi_i V_i\right) = 0 \quad \forall i = 1,\ldots,n \qquad (6)$$

$$\phi_L V_L + \phi V_{shr} = 0 \qquad V_{shr} = -D(\phi)\frac{\partial \phi}{\partial z}$$

$$\phi_L\left(V_L - V_{shr}\right) = -D\left(\phi_L\right)\frac{\partial \phi_L}{\partial_z} \qquad \Rightarrow V_L = \frac{\phi}{1-\phi} D(\phi)\frac{\partial \phi}{\partial z} \qquad (10)$$

$$D_{eff}(W) = D(W)\frac{\left(1 + \frac{\rho}{\rho_L} W_0\right)^2}{\left(1 + \frac{\rho}{\rho_L} W\right)^3} \qquad (15a)$$

$$V_{eff(s)}(W) = V_{rel(s)}(W)\left(\frac{1 + \frac{\rho}{\rho_L} W_0}{1 + \frac{\rho}{\rho_L} W}\right) \qquad (15b)$$

$$\frac{\partial}{\partial t}\left(\rho_L \phi_L\right) + \frac{\partial}{\partial z}\left(\rho_L \phi_L V_L\right) = -K_e \quad \text{(a) Liquid water}$$

$$\frac{\partial}{\partial t}\left(\rho_v \phi_{gas}\right) + \frac{\partial}{\partial z}\left(\rho_v \phi_{gas} V_v\right) = K_e \quad \text{(b) Vapor}$$

$$\frac{\partial}{\partial t}\left(\rho_{da} \phi_{gas}\right) + \frac{\partial}{\partial z}\left(\rho_{da} \phi_{gas} V_{da}\right) = 0 \quad \text{(c) Dry air} \qquad (18)$$

$$W = \frac{\rho_L \phi_L + \rho_v \phi_{gas}}{\rho \phi_c} \qquad (22)$$

$$\phi_{gas}(\text{Definition}) = 1 - \phi_c - \phi_L = 1 - \phi_c\left(1 + \frac{\rho}{\rho_L} W\right) \qquad (23)$$

$$D_{eff}(W) = D(W)\left(\frac{1 + \frac{\rho_s}{\rho_L} W_0}{1 + \frac{\rho_s}{\rho_L} W_c}\right)$$

$$-\rho \phi_0 \left(D_{eff}(W)\frac{\partial W}{\partial z_0}\right)_{z_0 = H_0} = F_m{}^d(t) \qquad (25)$$

$$(W)_{z_0 = 0} = W_g \quad \text{If } t < 1 \text{ hour}$$

$$-\rho \phi_0 \left[D_{eff}(W)\frac{\partial W}{\partial z_0}\right]_{z_0 = 0} \quad \text{If } t > 1 \text{ hour} \qquad (28)$$

$$f(\phi) = \left(\frac{\phi - \phi_g}{\phi_g}\right)^{k_1}, \; k_1 > 0 \quad \text{If } \phi < \phi_g$$

$$0 \quad \text{If } \phi > \phi_g \qquad (29)$$

$$f(\phi) = \left(\frac{\phi - \phi_c}{\phi_c}\right)^{1.3} \quad \text{If } \phi < \phi_c$$

$$0 \quad \text{If } \phi > \phi_c \qquad (30)$$